Perturbative analysis of simultaneous Stark and Zeeman effects on $n=1 \leftrightarrow n=2$ radiative transitions in positronium

C. D. Dermer
Physics Department, Lawrence Livermore National Laboratory, Livermore, California 94550

J. C. Weisheit
Department of Space Physics and Astronomy, Rice University, Houston, Texas 77251
(Received 19 July 1989)

Perturbative corrections to the wave functions of the 16 $n=2$ positronium states are used to derive the $n=1 \leftrightarrow n=2$ radiative transition rates of a positronium atom moving in arbitrarily oriented electric and magnetic fields. Excess annihilation radiation resulting from laser excitation and magnetic mixing in $n=2$ positronium is calculated and found to be in accord with a recent experiment.

I. INTRODUCTION

Experimental investigations of positronium (Ps) are of fundamental significance in testing quantum electrodynamics.[1] Studies of Ps are difficult because of its low mass and short ground-state lifetime (see Fig. 1 for lifetimes and energies of $n=1$ and $n=2$ Ps). Measurements of the $1\,^1S_0-1\,^3S_1$ fine-structure energy interval in ground-state Ps have employed magnetic quenching and microwave techniques.[1] Measurements in $n=2$ Ps include the $1\,^3S_1-2\,^3S_1$ transition,[2] observed using Doppler-free two-photon spectroscopy, and the $2\,^3S_1-2\,^3P_{0,1,2}$ transitions in orthopositronium (ortho-Ps),[3] which were observed by monitoring coincidences between Ly-α photons and annihilation radiation upon application of a resonant microwave field. Observation of the $1\,^3S-2\,^3P$ transitions in ortho-Ps with an incoherent light source has also been reported,[4] although the statistical significance of this study is low. To date, no measurements involving $n>2$ Ps states have been reported.

The accuracy of fine-structure measurements is limited by the Doppler effect: Ps atoms, when formed by thermal desorption methods,[5] have random velocities $v=\beta c \sim (1-2)\times 10^7$ cm/s, corresponding to temperatures ~ 1000 K. Production of cold Ps, such as through laser cooling,[6] will reduce this source of uncertainty. This technique requires that the $1\,^3S-2\,^3P$ transition of Ps be excited by broadband laser light (covering half the Ps Doppler profile) tuned to frequencies to the red of the $1\,^3S-2\,^3P$ transition frequency, using laser intensities near or above the optical saturation intensity. Optically saturated resonant excitation of the $1\,^3S-2\,^3P$ transition of Ps has recently been reported.[7] Excess annihilation radiation produced through magnetic mixing of ortho-Ps to parapositronium (para-Ps) in the $n=2$ state was used to demonstrate the optical saturation.

In the kinds of experiments described above, small electric and/or magnetic fields are often present. Previous theoretical work[8] on $n=2$ Ps gives exact diagonalizations of the 16×16 secular determinant for the energy levels of motional Ps in a magnetic field. These studies did not, however, include the effects of external electric fields, or consider radiative transitions between the $n=1$ and $n=2$ levels.

In this paper, we present a perturbative analysis of Zeeman and Stark effects from arbitrarily oriented electric and magnetic fields on radiative transitions between the $n=1$ and $n=2$ states of Ps. A rate equation ap-

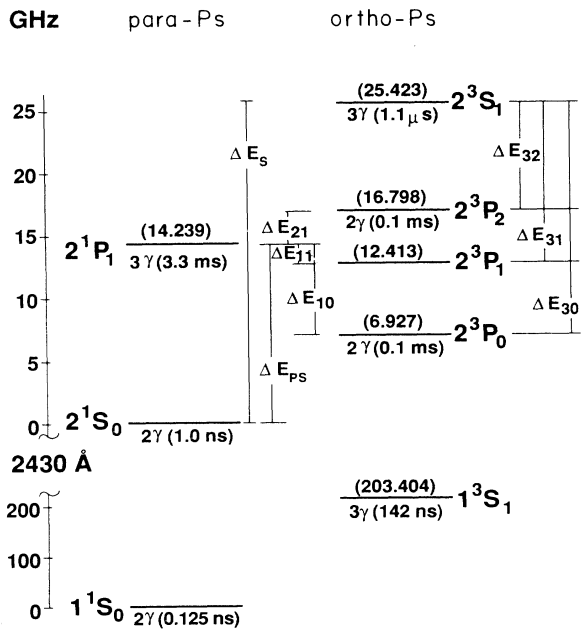

FIG. 1. Fine-structure energy levels and annihilation lifetimes of $n=1$ and $n=2$ Ps in the absence of external fields (see Ref. 1). Numbers in parentheses give relative energy of levels, including radiative corrections, in units of gigahertz. The spontaneous radiative lifetimes of the $2P$ and $2S$ levels are 3.2 ns and 0.24 s, respectively.

proach involving transitions between unperturbed ground-state wave functions and first-order perturbed excited-state ($n=2$) wave functions is used to calculate level populations and annihilation rates. The perturbative nature of the analysis limits magnetic fields to $\lesssim 300$ G, electric fields to $\lesssim 800$ V/cm, and Ps velocities to $\lesssim 10^8$ cm/s ($\beta \lesssim 0.003$).

II. ANALYSIS

A. Fields and transformations

We study radiative transitions between the ground ($n=1$) and lowest ($n=2$) excited states of Ps moving in arbitrarily oriented electric and magnetic fields. The geometry is shown in Fig. 2(a). The $\hat{\mathbf{z}}$ axis is along the direction of the magnetic field $\mathbf{B}$, and the vector $\boldsymbol{\beta}=\mathbf{v}/c$ is chosen to be in the $\hat{\mathbf{x}}$-$\hat{\mathbf{z}}$ plane. The polar and azimuthal angles of the electric field $\mathcal{E}$ and photon wave vector $\mathbf{k}$ are denoted by $\theta_{\mathcal{E}}$ and $\phi_{\mathcal{E}}$, and $\theta_{\mathbf{k}}$ and $\phi_{\mathbf{k}}$, respectively. Because the typical Ps $\beta \sim 3\times 10^{-4}$, we can neglect terms of order β^2 in the field transformations to the Ps rest frame. We also neglect the change in photon polarization, energy, and direction resulting from the boost, since the Ps atoms are moving at nonrelativistic velocities. For a characteristic electric field $\mathcal{E} \sim 50$ V/cm, the motional magnetic field $\sim 50\ \mu$G when $v \sim 10^7$ cm/s, and is negligible compared with typical magnetic field strengths considered here. When $B=100$ G, however, a motional Stark field ~ 10 V/cm is produced in the Ps rest frame and it cannot, in general, be neglected. The transformed fields in the Ps rest frame are therefore given to good approximation by

$$\mathbf{B}'=\mathbf{B}=B\hat{\mathbf{z}}, \quad \mathcal{E}'=\mathcal{E}-\beta_x B\hat{\mathbf{y}} . \tag{1}$$

If we now orient the axes in the Ps rest frame so that the transformed electric field is in the $\hat{\mathbf{x}}'$-$\hat{\mathbf{z}}'$ plane, we obtain the geometry shown in Fig. 2(b). This coordinate system is simplest for calculating perturbative corrections to the Ps wave functions. Here the component of $\mathcal{E}'$ parallel to $\mathbf{B}$ is denoted by $\mathcal{E}_{\parallel}=\mathcal{E}_z$, and the component of $\mathcal{E}'$ perpendicular to $\mathbf{B}$ (aligned along the $\hat{\mathbf{x}}'$ axis) is denoted by $\mathcal{E}_{\perp}=[\mathcal{E}_x^2+(\mathcal{E}_y-\beta_x B)^2]^{1/2}$. Note that the polar angle of $\mathbf{k}$ is $\theta_k'=\theta_k$, and that the azimuthal angle of $\mathbf{k}$ with respect to the x' axis is now given by $\phi_k'=\phi_k-\phi_{\mathcal{E}'}$, where

$$\tan\phi_{\mathcal{E}'}=(\mathcal{E}_y-\beta_x B)/\mathcal{E}_x . \tag{2}$$

The spherical polar angles (θ_k',ϕ_k') of $\mathbf{k}$ can be related to standard Euler angles of rotation. These, in turn, are needed to calculate the electric dipole transition rates for various polarization states of an emitted or absorbed photon.

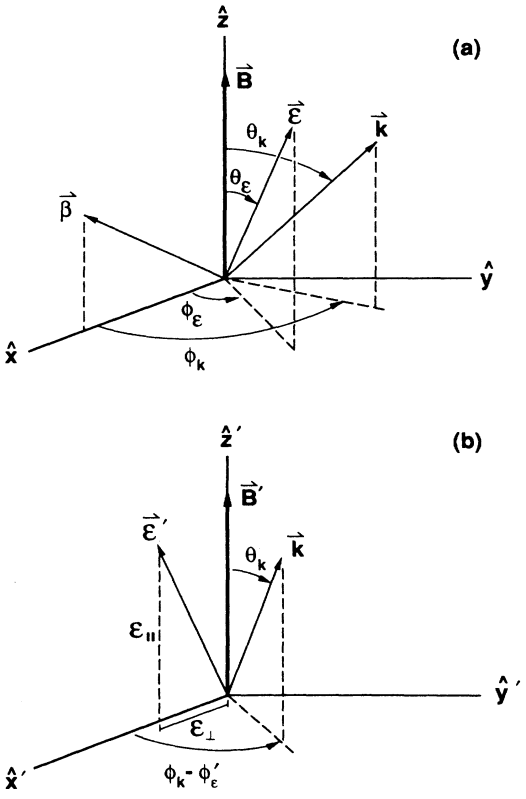

FIG. 2. (a) Coordinates for Ps in the laboratory frame, and (b) in a frame in which the Ps is at rest.

B. Perturbation equations

Our perturbing Hamiltonian is the sum of Zeeman- and Stark-effect terms,[8] and is given by

$$\tilde{H}=H_B+H_{\mathcal{E}}=-\boldsymbol{\mu}\cdot\mathbf{B}-e\mathcal{E}\cdot\mathbf{r}$$
$$\cong\mu_B B(\sigma_{1z}-\sigma_{2z})-er(\mathcal{E}_{\parallel}\cos\theta+\mathcal{E}_{\perp}\sin\theta\cos\phi) . \tag{3}$$

Here, $\mathbf{r}=(r,\theta,\phi)$ is the position of the positron relative to the electron, σ_{1z} and σ_{2z} are the Pauli operators for the z component of spin angular momentum for the electron and positron, respectively, and μ_B is the Bohr magneton ($\mu_B/h=1.40$ MHz/G). Note that the Zeeman factor proportional to $\mathbf{L}$, which appears in the familiar expression for H_B for ordinary atoms, vanishes in the case of Ps.

In the L-S coupling scheme, quantum numbers $\{\gamma\}=\{nSLJM\}$ completely specify each unperturbed Ps eigenstate. The 16 states having principal quantum number $n=2$ are listed in Table I, along with their decomposition into products of spin functions χ_{SM_S} and orbital (spherical harmonic) functions Y_{LM_L}. First-order corrected eigenstates (denoted by a tilde) for Ps atoms in the presence of the perturbing fields are given by the usual formula,

$$|\tilde{\gamma}\rangle=|\gamma\rangle-\sum_{\gamma'(\neq\gamma)}\frac{|\gamma'\rangle\langle\gamma'|\tilde{H}|\gamma\rangle}{E_{\gamma'}-E_{\gamma}} , \tag{4}$$

where the E_{γ} are unperturbed energy eigenvalues. Because of the relatively small separations $\Delta E_{\gamma'\gamma}=E_{\gamma'}-E_{\gamma}$ between fine-structure states of the same principal quantum number, the summation in Eq. (4) can be restricted to just those nearby states. Moreover, because the fine-structure splitting (203 GHz) between the sublevels of $n=1$ Ps is much greater than the fine-structure splitting

TABLE I. Perturbative corrections to the $n=2$ positronium wave functions.

$^1S_{00}$	$Y_{00}\chi_{00}$	$^1S_{00}-\varepsilon_S\,{}^3S_{10}-\varepsilon_{PS}(^1P_{11}-{}^1P_{1-1}-\rho\,{}^1P_{10})$
$^1P_{11}$	$Y_{11}\chi_{00}$	$^1P_{11}-2^{-1/2}(\varepsilon_{11}\,{}^3P_{11}+\varepsilon_{21}\,{}^3P_{21})+\varepsilon_{PS}\,{}^1S_{00}$
$^1P_{10}$	$Y_{10}\chi_{00}$	$^1P_{10}-3^{-1/2}(\varepsilon_{10}\,{}^3P_{00}+2^{1/2}\varepsilon_{21}\,{}^3P_{20})-\varepsilon_{PS}\rho\,{}^1S_{00}$
$^1P_{1-1}$	$Y_{1-1}\chi_{00}$	$^1P_{1-1}+2^{-1/2}(\varepsilon_{11}\,{}^3P_{1-1}-\varepsilon_{21}\,{}^3P_{2-1})-\varepsilon_{PS}\,{}^1S_{00}$
$^3S_{11}$	$Y_{00}\chi_{11}$	$^3S_{11}-\varepsilon_{32}(6^{-1/2}\,{}^3P_{20}+2^{-1/2}\rho\,{}^3P_{21}-{}^3P_{22})$ $-2^{-1/2}\varepsilon_{31}(\rho\,{}^3P_{11}+{}^3P_{10})-3^{-1/2}\varepsilon_{30}\,{}^3P_{00}$
$^3S_{10}$	$Y_{00}\chi_{10}$	$^3S_{10}+\varepsilon_S\,{}^1S_{00}+2^{-1/2}\varepsilon_{32}({}^3P_{21}-2\cdot3^{-1/2}\rho\,{}^3P_{20}-{}^3P_{2-1})$ $-2^{-1/2}\varepsilon_{31}({}^3P_{11}+{}^3P_{1-1})+3^{-1/2}\varepsilon_{30}\rho\,{}^3P_{00}$
$^3S_{1-1}$	$Y_{00}\chi_{1-1}$	$^3S_{1-1}+\varepsilon_{32}(6^{-1/2}\,{}^3P_{20}-2^{-1/2}\rho\,{}^3P_{2-1}-{}^3P_{2-2})$ $+2^{-1/2}\varepsilon_{31}(\rho\,{}^3P_{1-1}-{}^3P_{10})+3^{-1/2}\varepsilon_{30}\,{}^3P_{00}$
$^3P_{22}$	$Y_{11}\chi_{11}$	$^3P_{22}-\varepsilon_{32}\,{}^3S_{11}$
$^3P_{21}$	$2^{-1/2}(Y_{11}\chi_{10}+Y_{10}\chi_{11})$	$^3P_{21}+2^{-1/2}[\varepsilon_{21}\,{}^1P_{11}+\varepsilon_{32}(\rho{}^3S_{11}-{}^3S_{10})]$
$^3P_{20}$	$6^{-1/2}(Y_{11}\chi_{1-1}+2Y_{10}\chi_{10}+Y_{1-1}\chi_{11})$	$^3P_{20}+6^{-1/2}[2\varepsilon_{21}\,{}^1P_{10}+\varepsilon_{32}({}^3S_{11}-{}^3S_{1-1}+2\rho\,{}^3S_{10})]$
$^3P_{2-1}$	$2^{-1/2}(Y_{1-1}\chi_{10}+Y_{10}\chi_{1-1})$	$^3P_{2-1}+2^{-1/2}[\varepsilon_{21}\,{}^1P_{1-1}+\varepsilon_{32}(\rho\,{}^3S_{1-1}+{}^3S_{10})]$
$^3P_{2-2}$	$Y_{1-1}\chi_{1-1}$	$^3P_{2-2}+\varepsilon_{32}\,{}^3S_{1-1}$
$^3P_{11}$	$2^{-1/2}(Y_{10}\chi_{11}-Y_{11}\chi_{10})$	$^3P_{11}+2^{-1/2}[\varepsilon_{11}\,{}^1P_{11}+\varepsilon_{31}(\rho\,{}^3S_{11}+{}^3S_{10})]$
$^3P_{10}$	$2^{-1/2}(Y_{1-1}\chi_{11}-Y_{11}\chi_{1-1})$	$^3P_{10}+2^{-1/2}\varepsilon_{31}({}^3S_{11}+{}^3S_{1-1})]$
$^3P_{1-1}$	$2^{-1/2}(Y_{1-1}\chi_{10}-Y_{10}\chi_{1-1})$	$^3P_{1-1}-2^{-1/2}[\varepsilon_{11}\,{}^1P_{1-1}+\varepsilon_{31}(\rho\,{}^3S_{1-1}-{}^3S_{10})]$
$^3P_{00}$	$3^{-1/2}(Y_{11}\chi_{1-1}-Y_{10}\chi_{10}+Y_{1-1}\chi_{11})$	$^3P_{00}+3^{-1/2}[\varepsilon_{10}\,{}^1P_{10}+\varepsilon_{30}({}^3S_{11}-\rho\,{}^3S_{10}-{}^3S_{1-1})]$

among the $n=2$ sublevels, corrections to the ground-state wave functions are neglected here.

The matrix element $\langle\chi_{S',M_{S'}}|\sigma_{1z}-\sigma_{2z}|\chi_{S,M_S}\rangle$ is nonzero only when $M_S=M_{S'}=0$ and $S\neq S'$, so the magnetic perturbation only connects ortho and para states with the same values of n and z component of angular momentum, $M\hbar$. Zeeman matrix elements between ortho and para states of Ps are given by the general expression

$$\langle\gamma'|\tilde{H}_B|\gamma\rangle=\delta_{n'n}\delta_{L'L}\delta_{M'M}(-1)^{L+M}[(-1)^{S+S'}-1]\mu_B B \times\sqrt{3(2J'+1)(2J+1)}\begin{pmatrix}J' & 1 & J\\ -M & 0 & M\end{pmatrix}\times\begin{Bmatrix}S' & L' & J'\\ J & 1 & S\end{Bmatrix}. \tag{5}$$

The electric field perturbation only connects states of the same multiplicity whose orbital angular momenta differ by unity. The general expression for Stark matrix elements for Ps is

$$\langle\gamma'|\tilde{H}_{\mathcal{E}}|\gamma\rangle=\delta_{S'S}(-1)^{S+1+M'}e(n'L'|r|nL)\begin{Bmatrix}S' & L' & J'\\ 1 & J & L\end{Bmatrix}\times\sqrt{\max(L',L)(2J'+1)(2J+1)/2}\times\sum_q\tau_q\begin{pmatrix}J' & 1 & J\\ -M' & q & M\end{pmatrix}, \tag{6}$$

where $(n'L'|r|nL)$ is the radial matrix element, and τ is a vector with spherical components $\tau_{+1}=+\mathcal{E}_\perp$, $\tau_{-1}=-\mathcal{E}_\perp$, and $\tau_0=-2^{1/2}\mathcal{E}_\parallel$.

Using the results of Eqs. (5) and (6) in Eq. (3), we obtain the first-order perturbation corrections to the $n=2$ wave functions. These are listed in Table I in terms of the unperturbed angular momentum eigenstates, using the notation

$$\varepsilon_{\gamma'\gamma}=2\mu_B B/\Delta E_{\gamma'\gamma},\quad \gamma'\gamma=21,11,10,S\ ; \tag{7a}$$

$$\varepsilon_{\gamma'\gamma}=3\cdot2^{1/2}ea_0\mathcal{E}_\perp/\Delta E_{\gamma'\gamma},\quad \gamma'\gamma=PS,32,31,30\ ; \tag{7b}$$

$$\rho=2^{1/2}\mathcal{E}_\parallel/\mathcal{E}_\perp\ . \tag{7c}$$

The energy differences $\Delta E_{\gamma'\gamma}$ can be obtained from the values given in Fig. 1.

C. Rates of radiative transitions between $n=1$ and $n=2$ states of positronium

The rate of decay from one perturbed Ps state to another follows from the general theory of radiative transitions in atoms,[9] viz.,

$$dW_\sigma(\tilde{\gamma}',\tilde{\gamma})=(N_{\mathbf{k},\sigma}+1)(2k^3/3\hbar)|\hat{\mathbf{P}}_\sigma\cdot\langle\tilde{\gamma}'|\mathbf{d}|\tilde{\gamma}\rangle|^2 d\Omega_{\mathbf{k}}\ . \tag{8}$$

Here, $\mathbf{d}=+e\mathbf{r}$ is the Ps dipole moment, $\hat{\mathbf{P}}_\sigma$ is a unit vector that specifies the polarization σ of the photon with energy $\hbar\omega=\hbar ck$, emitted into a differential solid angle $d\Omega_{\mathbf{k}}$ about $\mathbf{k}$, and $N_{\mathbf{k},\sigma}$ is the number of ambient photons in mode $(\mathbf{k},\sigma)$. When no resonant radiation is present, Eq. (8) can be integrated over emission angle and summed over the two independent polarization states to yield the spontaneous rate $A(\gamma',\gamma)$. For dipole-allowed transitions $\gamma'\rightarrow\gamma$, we ignored all first-order corrections and adopted the spontaneous rate between unperturbed states,

$$A(\tilde{\gamma}',\tilde{\gamma}) \rightarrow A(\gamma',\gamma) \quad \text{(allowed)} . \tag{9a}$$

For dipole-forbidden transitions $\gamma' \rightarrow \gamma$, we used

$$A(\tilde{\gamma}',\tilde{\gamma}) \rightarrow \left[\frac{4k^3}{3\hbar}\right] \sum_q \left| \sum_{\gamma''(\neq\gamma')} \frac{\langle\gamma'|\tilde{H}|\gamma''\rangle\langle\gamma''|d_q|\gamma\rangle}{(E_{\gamma''}-E_{\gamma})} \right|^2 \quad \text{(forbidden)} . \tag{9b}$$

Spontaneous transition rates between the 16 substates of $n=2$ Ps and the four substates of $n=1$ Ps were evaluated from Eqs. (9) using the wave functions of Table I. In the analysis that follows, we found it convenient to use the fact that each rate between these perturbed substates is proportional to the (unperturbed) Ps term A value

$$A(2p,1s)=3.14\times10^8\ \text{s}^{-1} . \tag{10}$$

The individual proportionality factors are given in Table II. In the absence of electric and magnetic fields (i.e., when all $\varepsilon_{\gamma'\gamma}\rightarrow 0$), we recover the usual spontaneous-emission coefficients between specific magnetic substates. In the presence of a magnetic field, transitions between $1\,^3S$ and $2\,^1P$ states and between $2\,^3P$ and $1\,^1S$ states are possible. Transitions between the $1\,^3S$ and $2\,^3S$ states and between the $2\,^1S$ and $1\,^1S$ states are permitted by the Stark effect. To this order of perturbation theory, however, the Stark mixing between the $2S$ and $2P$ states results entirely from the electric field parallel to the direction of the magnetic field, so that motional Stark fields do not induce this mixing. Also, it may be noted that only one value of $q=\Delta M=M'-M$ contributes to each transition under consideration; this is indicated by the subscript $(\cdots)_q$, where $q=+$, 0, or $-$ for each entry in Table II.

Radiative transitions induced by polarized light incident from arbitrary angles can be calculated from Eq. (8), once the spherical components $(P_+,P_0,P_-)_\sigma$ of the polarization vector are determined in the Ps rest frame. Because only one value of $q=\Delta M$ contributes to each of the radiative transitions considered here, each induced rate is simply proportional to the appropriate P_q^2. In this paper we consider two situations, both with the incident photon propagation vector $\mathbf{k}\perp\mathbf{B}$. For light polarized linearly along $\mathbf{B}$, one has $P_q^2=(0,1,0)$, and for right-hand circularly polarized light, $P_q^2=(\frac{1}{4},\frac{1}{2},\frac{2}{4})$.

D. Saturation intensity

We define the saturation specific intensity J_ν^{sat} as the value of J_ν ($\text{J cm}^{-2}\text{s}^{-1}\text{Hz}^{-1}\text{sr}^{-1}$) giving a steady-state population of the upper level equal to one-half the population of the lower level. If J_ν varies slowly over the natural linewidth of a transition,

$$J_\nu^{\text{sat}}=\frac{A(\gamma',\gamma)}{2B(\gamma',\gamma)}=\frac{h\nu^3}{c^2} , \tag{11}$$

where ν is the frequency of the transition, and $A(\gamma',\gamma)$ and $B(\gamma',\gamma)$ are the Einstein coefficients for the transition from the upper to the lower state. According to this definition, the induced rate is one-half the spontaneous rate at saturation intensity.

The saturation energy flux required to irradiate a sample of atoms at saturation intensity depends on the frequency bandwidth $\Delta\nu$ of the laser through the relation $F_{\text{sat}}=4\pi J_\nu^{\text{sat}}\Delta\nu$. For the $1\,^3S-2\,^3P$ transition of Ps, $F_{\text{sat}}=8840\ \Delta\lambda\ \text{J cm}^{-2}\text{s}^{-1}$, where $\Delta\lambda$ is the bandwidth of the laser in angstroms. Thus irradiating a sample of Ps atoms at saturation intensity for 10 ns with a 1-Å bandwidth laser having a 1-cm^2 spot size requires $\sim 88\ \mu$J of energy.

TABLE II. Perturbative corrections to electric dipole transitions rates between $n=1$ and $n=2$ levels of positronium. All bank entries are zero. Subscript gives value of ΔM for the transition.

	$1\,^3S_{11}$	$1\,^3S_{10}$	$1\,^3S_{1-1}$	$1\,^1S_{00}$
$2\,^1S_{00}$				$\rho^2\varepsilon_{PS\,0}^2$
$2\,^1P_{11}$	$(\varepsilon_{11}+\varepsilon_{21})^2/4_0$	$(\varepsilon_{21}-\varepsilon_{11})^2/4_+$		1_+
$2\,^1P_{10}$	$(\varepsilon_{10}+\varepsilon_{21})^2/9_-$	$(\varepsilon_{10}-2\varepsilon_{21})^2/9_0$	$(\varepsilon_{10}+\varepsilon_{21})^2/9_+$	1_0
$2\,^1P_{1-1}$		$(\varepsilon_{21}-\varepsilon_{11})^2/4_-$	$(\varepsilon_{11}+\varepsilon_{21})^2/4_0$	1_-
$2\,^3S_{11}$	$\rho^2(\varepsilon_{31}+\varepsilon_{32})^2/4_0$	$\rho^2(\varepsilon_{32}-\varepsilon_{31})^2/4_+$		
$2\,^3S_{10}$	$\rho^2(\varepsilon_{32}-\varepsilon_{30})^2/9_-$	$\rho^2(\varepsilon_{30}+2\varepsilon_{32})^2/9_0$	$\rho^2(\varepsilon_{32}-\varepsilon_{30})^2/9_+$	
$2\,^3S_{1-1}$		$\rho^2(\varepsilon_{32}-\varepsilon_{31})^2/4_-$	$\rho^2(\varepsilon_{31}+\varepsilon_{32})^2/4_0$	
$2\,^3P_{22}$	1_+			
$2\,^3P_{21}$	$\frac{1}{2}0$	$\frac{1}{2}+$		$\varepsilon_{21}^2/2_+$
$2\,^3P_{20}$	$\frac{1}{6}-$	$\frac{2}{3}0$	$\frac{1}{6}+$	$2\varepsilon_{21}^2/3_0$
$2\,^3P_{2-1}$		$\frac{1}{2}-$	$\frac{1}{2}0$	$\varepsilon_{21}^2/2_-$
$2\,^3P_{2-2}$			1_-	
$2\,^3P_{11}$	$\frac{1}{2}0$	$\frac{1}{2}+$		$\varepsilon_{11}^2/2_+$
$2\,^3P_{10}$	$\frac{1}{2}-$		$\frac{1}{2}+$	
$2\,^3P_{1-1}$		$\frac{1}{2}-$	$\frac{1}{2}0$	$\varepsilon_{11}^2/2_-$
$2\,^3P_{00}$	$\frac{1}{3}-$	$\frac{1}{3}0$	$\frac{1}{3}+$	$\varepsilon_{10}^2/3_0$

III. NUMERICAL RESULTS

We calculated the time-dependent populations of the 20 $n=1$ and $n=2$ Ps states due to the application of an external laser field, using the annihilation rates and lifetimes given in Fig. 1, and the transition rates between the various levels given in Table II. The transition rates from each perturbed $2P$ level to the unperturbed $1S$ levels were all reduced by a common factor so that their sum would yield the term value $A(2p,1s)$. The radiative transition rates from the perturbed $2S$ states to the $1S$ states are well approximated by the values in Table II, since the radiative lifetimes for the unperturbed $2S \leftrightarrow 1S$ transitions ($\cong 0.24$ s) are even longer than their annihilation lifetimes. The laser time profile was characterized by a Gaussian function with 10 ns full width at half maximum (FWHM) intensity centered at $t=20$ ns.

The results of a numerical simulation of the time dependence of the Ps level populations with $B=200$ G and $\mathcal{E}_{\parallel}=50$ V/cm ($\mathcal{E}_x=\mathcal{E}_y=0$) are shown in Fig. 3. The laser energy I and bandwidth $\Delta\lambda$ are 100 μJ and 0.65 Å, respectively. The laser was taken to be linearly polarized along the direction of the magnetic field with $\mathbf{k}\perp B$, and the Ps were assumed to be traveling with a velocity of 10^7 cm/s at an angle of 45° with respect to the direction of the magnetic field. The initial Ps population $N_{\rm Ps}(t=0)=1$, and was divided equally among the three $1\,^3S_1$ states. As can be seen, the laser irradiation causes

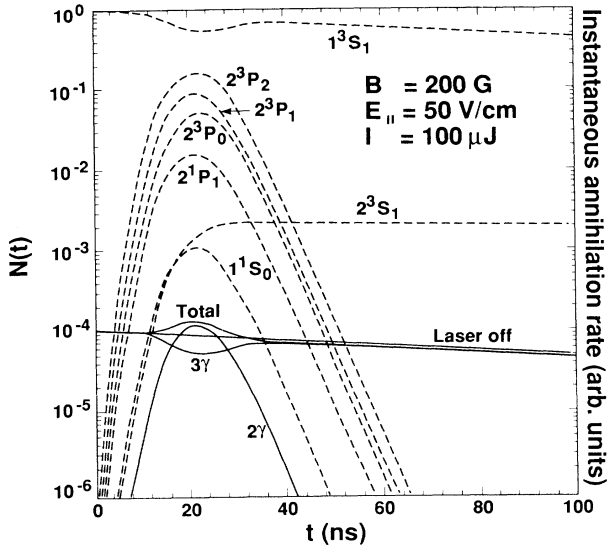

FIG. 3. Time-dependent level populations $N(t)$ of Ps irradiated by a 2430-Å laser with 0.65 Å bandwidth (dashed curves), and instantaneous annihilation rates (solid curves). The energy of the laser pulse is 100 μJ, and the laser intensity time profile is given by a 10-ns FWHM Gaussian function centered at 20 ns. Ps energy levels, shown by the dashed curves, are denoted by the unperturbed state labels. The magnetic field $B=200$ G and the parallel electric field $\mathcal{E}_{\parallel}=50$ V/cm. The radiation is linearly polarized along the direction of the magnetic field, and the Ps are assumed to travel at an angle of 45° with respect to the direction of B with a velocity of 10^7 cm/s.

the populations of the $n=2$ states to increase at the expense of the $1\,^3S_1$ population until the laser power starts to decrease at $t=20$ ns. The asymmetry of the $n=2$ populations about $t=20$ ns arises from the continual loss of Ps from the system due to annihilation, and from the 3.2-ns radiative decay lifetime of the $2P$ level after the laser light has effectively turned off. Also, a small fraction of Ps reaching the $2\,^3S_1$ level through Stark mixing remains trapped in this state long after the laser irradiation has ceased.

The solid curves in Fig. 3 are proportional to the instantaneous annihilation rates of Ps. The curve labeled "Laser off" shows the annihilation rate in the absence of laser excitation. The curve labeled "3γ" shows the annihilation rate from the $1\,^3S_1$ state and, to a much lesser extent, the $2\,^3S_1$ states. The curve labeled "2γ" shows the annihilation rate from the $1\,^1S_0$ and $2\,^1S_0$ states resulting from transitions between ortho and para states induced by the Zeeman effect. Annihilation from $2P$ states is small and neglected. The net annihilation rate is shown by the curve labeled "Total," in which ortho-Ps 3γ annihilations are given $\frac{3}{2}$ times the weight as para-Ps 2γ annihilations. This assumes that the detector has equal sensitivity to 2γ and 3γ decay, which may not be true in practice because of the differences in the ortho-Ps and para-Ps annihilation spectra.

By integrating the annihilation signal over a fixed time interval, we find that Zeeman mixing in the $n=2$ levels and subsequent annihilation from the $1\,^1S_0$ level can lead to an annihilation rate in excess of the rate which occurs for the same system when the laser is off. We define the fractional excess annihilation radiation produced by laser illumination of an ortho-Ps sample during a time interval of length Δt by the expression

$$f_{\rm ex}=[(2\eta_{2\gamma}/3+\eta_{3\gamma})/\eta_{\Delta t}]-1\ , \tag{12}$$

where $\eta_{2\gamma}$ and $\eta_{3\gamma}$ are the fractions of Ps that annihilate into two and three photons in time Δt, respectively, and $\eta_{\Delta t}=1-\exp(-\Delta t/\tau_{\text{ortho-Ps}})$ is the ortho-Ps decay fraction in the absence of laser illumination. For example, in the 40-ns window centered about the peak of the laser time profile at $t=20$ ns, an excess annihilation radiation fraction of 12.8% is calculated for the parameters of Fig. 3. This effect is used elsewhere[7] to demonstrate resonant excitation and optical saturation of the $1S-2P$ transition in Ps.

Figure 4 shows another simulation with $\mathcal{E}_{\parallel}$ and I increased to 500 V/cm and 500 μJ, respectively. The magnitude of the excess annihilation signal in the 40-ns window centered at $t=20$ ns has increased to 24.3%, with a larger fraction of the Ps remaining in the $2\,^3S$ state at long times ($t>40$ ns) compared with the values plotted in Fig. 3. The rate at which Ps atoms in the $2\,^3S$ state spontaneously decay to the $1\,^3S$ state increases as a result of the increased Stark mixing, so that the Ps atoms do not remain in the $2\,^3S$ as long as in the case illustrated in Fig. 3. Thus one needs lower laser energies to excite a given fraction of Ps to the long-lived $2\,^3S_1$ states when $\mathcal{E}_{\parallel}$ is larger, but as a consequence the lifetime of that state decreases.

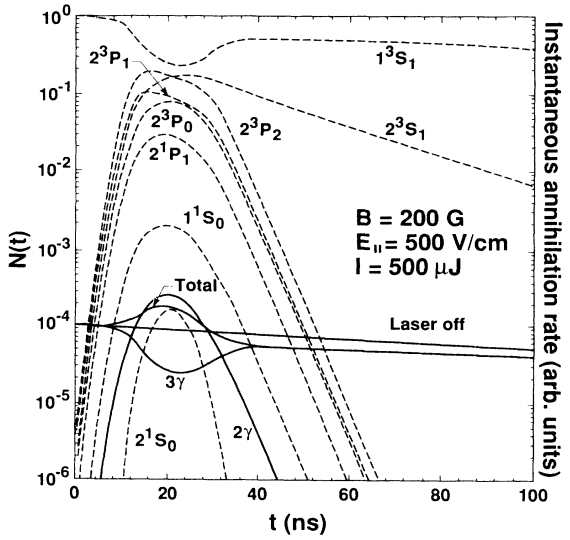

FIG. 4. Same as Fig. 3, but with a laser pulse energy of 500 μJ and with $\mathcal{E}_{\parallel}=500$ V/cm.

The calculated fractional excess annihilation radiation in a 40-ns window centered at the peak of the laser time profile is shown in Fig. 5 as a function of I, again with $\Delta\lambda=0.65$ Å. Results are shown for linearly and circularly polarized light with $\mathbf{k}\perp\mathbf{B}$, $B=200$ G, and $\mathcal{E}_{\parallel}=50$ V/cm. Values of f_{ex} are smaller in the case of circularly polarized light than in the case of linearly polarized light, because in the former case the electric dipole-matrix elements connect states that are not mixed through the Zeeman effect, for example, in the transition $1\,^3S_{11}\leftrightarrow 2\,^3P_{22}$. For a laser pulse energy of 100 μJ, we find that the ratio of f_{ex} for circularly polarized light relative to linearly polarized light is 0.36, as compared with the experimental ratio of 0.42 ± 0.2.[7]

As I increases, f_{ex} approaches an asymptotic value as the ortho-Ps mix into para states, annihilate, and thereby deplete the total population of Ps atoms. For $\Delta t=40$ ns, $f_{ex}(I\rightarrow\infty)\rightarrow 1.72$, from Eq. (12). One can roughly

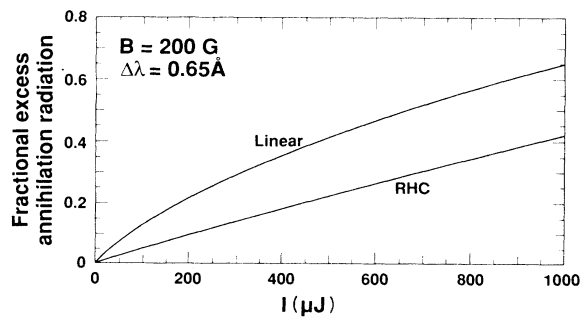

FIG. 5. Fractional excess annihilation radiation as a function of laser pulse energy in a 40-ns window centered at the peak of the laser time profile. All other parameters are as given in Fig. 3. Cases shown are for right-hand circularly polarized laser light, and for linearly polarized light with the polarization vector parallel to B. The photon propagation vector $\mathbf{k}\perp\mathbf{B}$.

determine the laser power at which $\sim\frac{1}{2}$ the Ps atoms are depleted through mixing by an expression of the form $(1-\varepsilon^2)^N\approx\frac{1}{2}$, where ε is a characteristic Zeeman mixing coefficient and $N=\delta t/t_{cyc}$ is the average number of times a Ps atom will cycle between the $n=1$ and $n=2$ states in time δt, the duration of laser illumination. In the fully optically saturated limit, that is, when $J_\nu/J_\nu^{sat}\gg 1$, the cycling time $t_{cyc}\rightarrow 2/B_{21}J_\nu$. For $B=200$ G, $\Delta E\sim 2.5$ GHz, and $\Delta\lambda=0.65$ Å, depletion of $\sim 50\%$ of the Ps in ~ 10 ns will occur when $I\sim 1000$ μJ. This description of excess annihilation radiation is in good accord with experimental observations.[7]

IV. DISCUSSION

Count rates of annihilation photons can be used to monitor excitation of Ps to the $n=2$ level. When Ps atoms are produced in a pulsed fashion, as in the Lawrence Livermore National Laboratory Linac,[5,7] this is accomplished by comparing the time dependence of the annihilation count rate with no laser illuminating the Ps sample to the count rate when the laser is on. Without laser excitation, a prompt 2γ annihilation pulse is observed from Ps formed in the $1\,^1S$ state, followed by a residual 3γ annihilation background from $1\,^3S$ decay, which lasts for ~ 100 ns. The annihilation rate can either increase or decrease due to laser excitation of the Ps $1\,^3S\rightarrow 2\,^3P$ transition. A decrease in the relative annihilation signal will be observed for sufficiently weak magnetic fields, since excited Ps will spend time in the $2\,^3P$ level with an annihilation lifetime much longer than the 142-ns ground-state annihilation lifetime. When the magnetic field is strong enough to induce Zeeman mixing of ortho and para states in the $n=2$ states, annihilation of Ps from the $1\,^1S_0$ state can lead to an increase of the annihilation signal relative to the signal strength in the absence of laser excitation, as illustrated in Fig. 5.

Increased experimental sensitivity to laser excitation of the $n=2$ level can be achieved by using either two-photon coincidence detectors (Anger cameras) or high-resolution detectors to discriminate between 2γ and 3γ decay. As is well known, the ortho-Ps 3γ decay spectrum is a continuum extending to 0.511 MeV, whereas the photons emitted in the para-Ps 2γ decay each have discrete energies of 0.511 MeV in the Ps rest frame. Observation of 2γ decay coincident with laser irradiation of Ps tens of nanoseconds after the initial Ps production pulse would provide additional evidence for Zeeman mixing between the ortho and para states in $n=2$ Ps.

The effect of Zeeman mixing in $n=2$ Ps provides a method for producing a narrow 0.511-MeV line using a narrow-bandwidth 2430-Å laser to velocity-select Ps. The mixing will result in transitions to the $1\,^1S_0$ level from which a very narrow 0.511-MeV annihilation line will be emitted. This effect was overlooked in Ref. 10, invalidating Letokhov and Minogin's method for producing nearly monoenergetic annihilation γ radiation.

The ability to induce transitions from ortho-Ps to para-Ps is also important in other applications. (i) Using this effect to provide a source of narrow, time-variable 0.511-MeV line radiation, one can produce narrow,

frequency-tunable γ-ray line emission between 0.170 and 0.511 MeV in conjunction with a Compton-scattering γ-ray mirror.[11] (ii) The production of stimulated 0.511-MeV annihilation in the laboratory depends on a method for converting ortho-Ps to para-Ps. The application of 203-GHz microwaves has been suggested to achieve this conversion.[6] Zeeman mixing to para states following laser excitation of ortho-Ps to the $n=2$ states gives another method for doing this. (iii) The Zeeman effect in $n=2$ Ps also provides a method to map the velocity distribution of Ps. A narrow-bandwidth 2430-Å laser can be used to velocity select and excite a small fraction of Ps. Zeeman mixing in $n=2$ Ps will lead to an enhancement of 2γ annihilation photons proportional to the relative number of Ps having velocities in resonance with the applied radiation. By varying the laser frequency, different Ps velocity intervals will be excited by the radiation, from which a one-dimensional velocity profile can be derived.

This resonance excitation can also be used to diagnose laser cooling of Ps, but it is then necessary to use a laser with an intensity greatly in excess of optical saturation intensity. This is because cooling with a broadband 2430-Å laser requires intensities near or above the $1S$-$2P$ optical saturation intensity[6] and, at optical saturation intensity, B must be less than ~ 100 G (Ref. 12) in order that the ortho-para conversion via the Zeeman effect not interfere with cooling. The laser used to diagnose cooling must therefore be at even higher intensities so that Ps atoms cycle between the $1S$ and $2P$ states a sufficient number of times to produce an observable annihilation signal.

All of the above considerations presume that the electric field in the direction of B is small; otherwise, a substantial fraction of the Ps will be trapped in the long-lived $2\,^3S$ state. Indeed, we can expect a reduction in the fractional excess annihilation radiation observed as $\mathcal{E}_{\parallel}$ is made larger, due to increased Stark mixing from $2\,^3P$ to $2\,^3S$. The presence of Ps in the $2\,^3S$ state could be demonstrated by photoionizing the excited Ps atoms with a laser of wavelength $\lambda < 7290$ Å at long times following laser irradiation. The free electrons or positrons could then be detected with a microchannel plate.

Stark mixing of $2\,^3P$ and $2\,^3S$ states may be of particular interest in fine-structure measurements of $n=2$ Ps, as it could provide a method for populating the $2\,^3S$ states more efficiently than can be done through radiative recombination.[3] Two-photon excitation[2] can also, of course, populate the $2\,^3S$ states, but without the velocity selectivity possible with one-photon excitation. Velocity selection of Ps during excitation would reduce the Doppler motions of those Ps atoms "mixed" to the $2\,^3S$ level. This would in itself represent a first sample of Ps atoms cooled in one dimension, although with the loss of those Ps atoms not originally formed with low velocity in this direction. Fine-structure measurements of the $2\,^3S_1-2\,^3P_{0,1,2}$ intervals in a microwave cavity (taking into account Stark shifts on energies) could be monitored by a change in the annihilation radiation count rate as the frequency of the microwave radiation passes through the resonance frequency of the transition; this could represent one of the most sensitive tests of quantum electrodynamics available.

In summary, we have presented a perturbative analysis of the resonant excitation of Ps moving in arbitrarily oriented electric and magnetic fields. Mixing of ortho-Ps and para-Ps by the Zeeman effect in $n=2$ Ps, which changes the annihilation rate, can be used to monitor laser excitations of Ps atoms. This effect is of interest in connection with attempts to cool Ps and to measure the fine-structure energies in $n=2$ Ps. Finally, we find good agreement between our numerical calculations and recent experiments to optically saturate the Ps $1\,^3S-2\,^3P$ transition.

ACKNOWLEDGMENTS

We acknowledge many valuable conversations with R. H. Howell, F. Magnotta, and K. P. Ziock, and thank S. N. Dixit, P. O. Egan, J. C. Garrison, and E. P. Liang for useful comments. This work was performed under the auspices of the U.S. Department of Energy by the Lawrence Livermore National Laboratory under Contract No. W-7405-ENG-48.

[1] S. Berko and H. N. Pendleton, Ann. Rev. Nucl. Part. Sci. **30**, 543 (1980); A. Rich, Rev. Mod. Phys. **53**, 127 (1981).

[2] S. Chu, A. P. Mills, and J. L. Hall, Phys. Rev. Lett. **52**, 1689 (1984).

[3] A. P. Mills, S. Berko, and K. F. Canter, Phys. Rev. Lett. **34**, 1541 (1975); S. Hatamian, R. S. Conti, and A. Rich, *ibid.* **58**, 1833 (1987).

[4] S. L. Varghese, E. S. Ensberg, V. W. Hughes, and I. Lindgren, Phys. Lett. **49A**, 415 (1974).

[5] R. H. Howell, M. J. Fluss, I. J. Rosenburg, and P. Meyer, Nucl. Instrum. Methods Phys. Res. **B10/11**, 373 (1985); R. H. Howell, I. J. Rosenburg, and M. J. Fluss, Appl. Phys. A **43**, 247 (1987).

[6] E. P. Liang and C. D. Dermer, Opt. Commun. **65**, 419 (1988).

[7] K. P. Ziock, C. D. Dermer, R. H. Howell, F. Magnotta, and K. M. Jones, J. Phys. B (to be published).

[8] S. M. Curry, Phys. Rev. A **7**, 447 (1973); M. L. Lewis and V. W. Hughes, *ibid.* **8**, 625 (1973).

[9] I. I. Sobelman, *Atomic Spectra and Radiative Transitions* (Springer-Verlag, New York, 1979).

[10] V. S. Letokhov, Phys. Lett. **49A**, 275 (1974); V. S. Letokhov and V. G. Minogin, Zh. Eksp. Teor. Fiz. **71**, 135 (1976) [Sov. Phys.—JETP **44**, 70 (1976)].

[11] C. D. Dermer, J. Appl. Phys. (to be published).

[12] C. D. Dermer, in *Proceedings of a Workshop on Annihilation in Gases and Galaxies,* edited R. J. Drachman (NASA Conference Publication, Greenbelt, MD, in press).